Article

Bandgap Engineering in #-Extended Pyrroles. A Modular Approach to Electron-Deficient Chromophores with Multi-Redox Activity

Halina Zhylitskaya, Joanna Cybinska, Piotr Chmielewski, Tadeusz Lis, and Marcin St#pie#

Just Accepted

Bandgap Engineering in π-Extended Pyrroles. A Modular Approach to Electron-Deficient Chromophores with Multi-Redox Activity

Halina Zhylitskaya,[†] Joanna Cybińska,[†‡] Piotr Chmielewski,[†] Tadeusz Lis,[†] and Marcin Stępień[†*]

[†] Wydział Chemii, Uniwersytet Wrocławski, ul. F. Joliot-Curie 14, 50-383 Wrocław, Poland

[‡] Wrocławskie Centrum Badań EIT+, ul. Stabłowicka 147, 54-066 Wrocław, Poland

ABSTRACT: A family of bandgap-tunable pyrroles structurally related to rylene dyes was computationally designed and prepared using robust, easily scalable chemistry. These pyrroles show highly variable fluorescence properties and can be used as building blocks for the synthesis of electron-deficient oligopyrroles. The latter application is demonstrated through the development of π-extended porphyrins containing naphthalenediamide or naphthalenediimide units. These new macrocycles exhibit simultaneously tunable visible and near-IR absorptions, an ability to accept up to 8 electrons via electrochemical reduction, and high internal molecular free volumes. When chemically reduced under inert conditions, the most electron-deficient of these macrocycles revealed reversible formation of eight charged states, characterized by remarkably red-shifted optical absorptions, extending beyond 2200 nm. Such features make these oligopyrroles of interest as functional chromophores, charge-storage materials, and tectons for crystal engineering.

INTRODUCTION

The synthetic chemistry of large polycyclic heteroaromatic molecules (PHAs) has recently become an area of intense investigation, because of the relevance of such systems as heteroatom-doped analogues of nanographenes and graphene nanoribbons.[1,2] The prospective use of these molecules in organic electronics requires precise control over their π-conjugation, notably their frontier orbital energies and electronic bandgaps. The synthesis of extended PHA systems can in principle be simplified by employing a modular approach, in which suitably designed building blocks (monomers) are covalently assembled into larger fused structures. For maximum design flexibility, bandgap engineering should be performed on the building block level. However, such an approach requires not only efficient strategies of bandgap tuning but also a good understanding of the relationship between the electronic structure of the monomer and the properties of its oligomeric derivatives.

Systematic tuning of optical bandgaps[3] can be achieved by homologation (oligomerization) of linear π-conjugated motifs,[4] such as oligophenyls,[5,6] rylenes,[7–9] oligoporphyrins,[10,11] or BODIPY[12] derivatives, although in general, the bandgap narrowing effect weakens with the increasing oligomer length. A formally related strategy involves ring expansion of π-conjugated macrocycles,[13,14] but its predictability is limited by the complex conformational behavior of large rings.[15] A complementary approach relies on combining donor and acceptor (D–A) moieties, with diverse recent applications in small-molecule[16–21] and polymer chemistry.[22–25] The D–A method is particularly suitable for the development of tunable building blocks, which can be constructed by judicious merging of existing electron-deficient and electron-rich motifs.

A simple and potentially productive design of such a hybrid structure, consisting of naphthalenemonoimide (NMI, red) and pyrrole (blue), is proposed in Figure 1. NMI is the key constituent of perylenediimide (PDI)[26–28] and naphthalenediimide (NDI)[29] dyes, and is known to offer excellent chemical stability and diverse derivatization options, usually based acyl chemistry, heterocyclic annulation reactions,[30] and lateral ring fusion.[31] Structural modifications can be used to change the electron-withdrawing character of the naphthalene fragment, which thus can serve as a tunable acceptor unit.[32,33] Consequently, the NMI-based and related chromophores can be tailored for use in various fields of application, e.g. as n-channel OFETs,[34] or functional cavities.[35] Because the bandgap changes in such hybrid monomers are expected to be amplified upon oligomerization, the resulting pyrroles are of immediate interest as building blocks for small-molecule dyes, such as dipyrrins[36,37] or α-linked oligopyrroles,[38,39] as well as for pyrrole-based macrocycles,[40] nanographenoids,[41–44] and polymers.[22,45] The synthetic approach relying on tunable pyrrole monomers can thus be envisaged to complement the existing routes to directly fused rylene–oligopyrrole hybrids.[46–48]
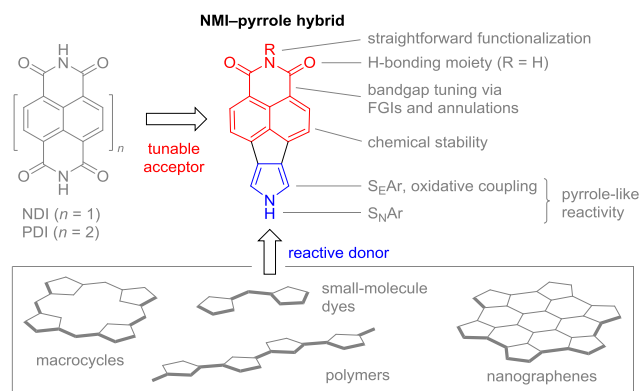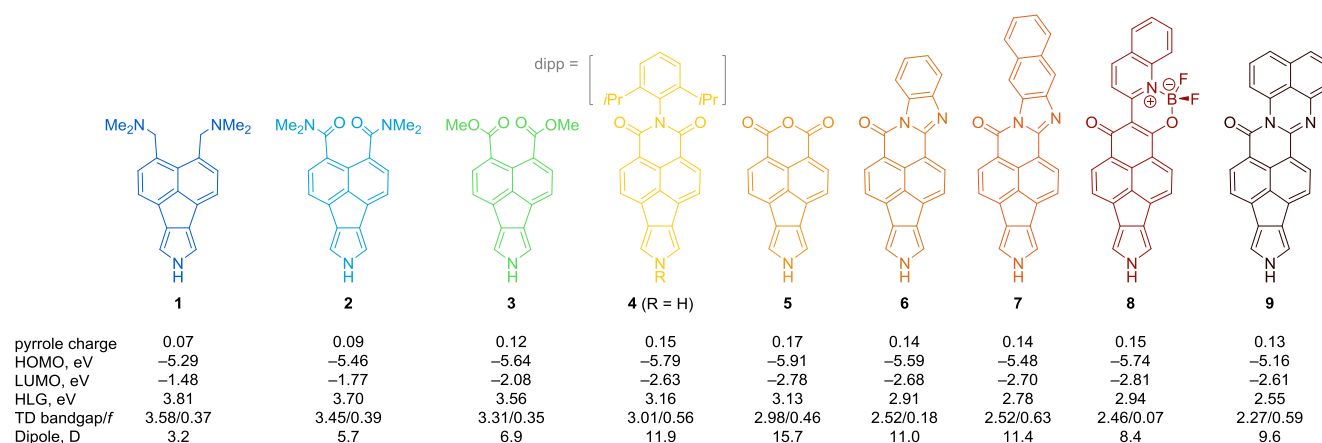
Figure 1. Design principle illustrated for the prototypic NMI–pyrrole hybrid. FGI, functional group interconversion, $S_{E(N)}Ar$ aromatic electrophilic (nucleophilic) substitution.

Chart 1. π-Extended Pyrrole Library[a]

pyrrole charge	0.07	0.09	0.12	0.15	0.17	0.14	0.14	0.15	0.13
HOMO, eV	−5.29	−5.46	−5.64	−5.79	−5.91	−5.59	−5.48	−5.74	−5.16
LUMO, eV	−1.48	−1.77	−2.08	−2.63	−2.78	−2.68	−2.70	−2.81	−2.61
HLG, eV	3.81	3.70	3.56	3.16	3.13	2.91	2.78	2.94	2.55
TD bandgap/f	3.58/0.37	3.45/0.39	3.31/0.35	3.01/0.56	2.98/0.46	2.52/0.18	2.52/0.63	2.46/0.07	2.27/0.59
Dipole, D	3.2	5.7	6.9	11.9	15.7	11.0	11.4	8.4	9.6

[a] Natural population (NPA) charges on the pyrrole rings, calculated Kohn–Sham HOMO, LUMO, and bandgap (HLG) energies, TDA bandgaps ($f > 0.05$), and oscillator strengths, dipole moments; all values calculated at the PCM(DMSO)/B3LYP/6-31G(d,p) level of theory. dipp = 2,6-di(isopropyl)phenyl.
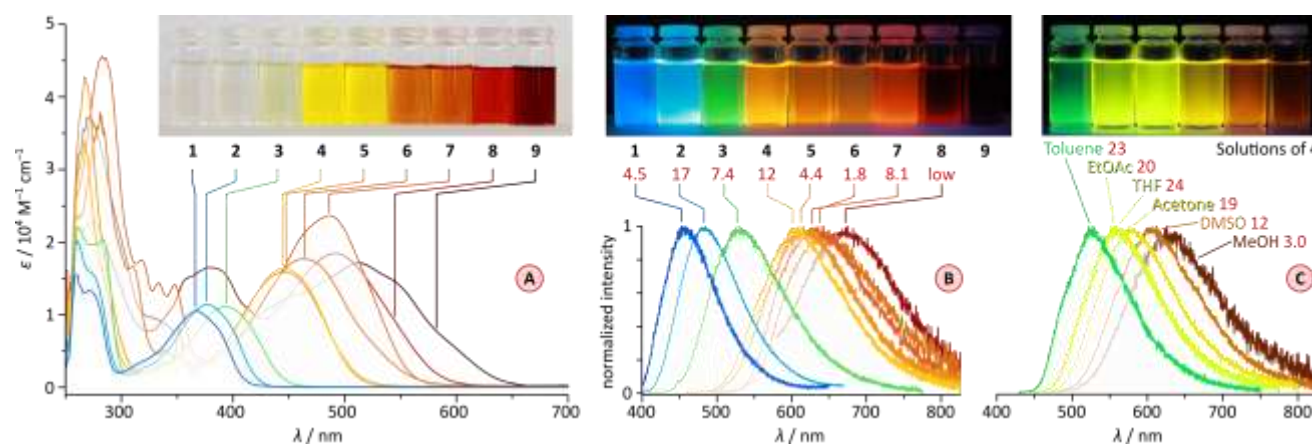
Because of the favorable combination of chemical stability and reactivity, these pyrroles are useful as covalent building blocks. This use is demonstrated here by the synthesis of π-extended porphyrin derivatives characterized by large curvatures and a remarkable multi-redox behavior.

RESULTS AND DISCUSSION

Pyrroles: Design and Synthesis. The design of the pyrrole library shown in Chart 1 was guided by DFT calculations, which provided theoretical estimates of HOMO–LUMO gaps (HLGs), from either Kohn–Sham (KS) orbital energies or TD-DFT excited-state calculations. It was found that, starting from compound **2**, the HLG could be progressively reduced by structural elaboration of the acceptor end of the fused pyrrole. Switching off the acceptor functionality by reduction of the amide groups was also considered (compound **1**), and was indeed predicted to result in a broadened HLG (3.81 eV),

Figure 2. Optical properties of pyrroles **1–9**. (**A**) Absorption spectra (~0.1 mM, DMSO, 293 K). (**B**) Fluorescence emission spectra (~5 μM, DMSO, 293 K). (**C**) Fluorescence solvatochromism of **4**. Fluorescence quantum yields (Φ_F, values in red) are given in %.

Here we show that by fusing pyrrole with electron-deficient naphthalene derivatives, it is possible to create a family of chromophores with tunable electronic characteristics.

comparable with those calculated for reported electron-rich systems, the unsubstituted acenaphthopyrrole[49–53] and its 2,5-di-*tert*-butyl derivative[54] (3.89 and 3.97 eV, respectively, at the

same level of theory). In **2**, the KS bandgap (3.70 eV) is comparable with that predicted for 3,4-dichloroacenaphthopyrrole[53,55] (3.64 eV). In pyrroles **2–5**, the reduction of the bandgap is achieved principally by the increasing electron-withdrawing effect of the functional groups, which is demonstrated by the progressive decrease of the KS HOMO and LUMO energies and by the increase of the partial charge residing on the pyrrole ring (Chart 1, Figure S37). In the small-bandgap derivatives **6–9**, the pyrrole partial charge and the LUMO energy vary over a narrow range and the decrease in HLG is caused by lifting of the HOMO levels, which can be attributed to the extension of the π system.

The preparative work was commenced with the synthesis of the diamide pyrrole **2** (Chart 1), which was obtained from acenaphthene in 6 steps (Supporting Information). The procedure, relying on the sulfone-Zard–Barton reaction[56] as the key step, is easily scalable, yielding multigram quantities of the product. The electron-withdrawing character of the amide groups in **2** provides sufficient stability to the fused pyrrole ring to permit chemoselective functionalization of the acceptor end of the molecule under a range of reaction conditions. Thus, by using straightforward transformations, a library of diversely functionalized pyrrole derivatives could be rapidly developed from **2** (Chart 1). Diamine **1**, imide **4**, and anhydride **5** were obtained respectively via LAH reduction (71%) and acid-catalyzed imidation (67%), and cyclization (82%). DBU-catalyzed MeI/MeOH cleavage of **5** produced diester **3** (82%). When condensed with appropriate aromatic diamines, **5** furnished imidazoles **6** (86%) and **7** (52%) and the fused pyrimidine **9** (79%). Finally, compound **8** was obtained in two steps[57] from **5**, quinaldine and boron trifluoride (42% overall yield). With the exception of **8**, which is prone to hydrolysis, the pyrroles show good to excellent chemical and photochemical stability. In particular, dilute solutions of **4–7** and **9** (e.g., 0.1 mM in DMSO) can be stored for weeks under ambient conditions with no significant decomposition.

Pyrroles: Structure and Optical Properties. Absorption measurements performed for **1–9** confirmed the qualitative validity of DFT calculations. The observed bathochromic shift of the lowest-energy absorption in the pyrroles (Figure 2A) was in agreement with the TD-DFT predicted bandgap variation (Chart 1), leading to a color progression from colorless through red-brown. Pyrroles **1–8** showed a weak-to-moderate fluorescence emission in DMSO solutions ($\Phi_F <$ 20%, Figure 2B), whose color varied from blue to red, tailing into the near-IR range for **6–8**. The fluorescence red shifts were found to correlate better with absorption onsets rather than with positions of absorption maxima. For **9**, weak fluorescence emission with $\lambda_{max}^{em} \approx 630$ nm was recorded in a DMSO solution (Figure S17). The fluorescence quantum yield of **4** did not improve upon N-substitution (**4'**, R = CH$_2$CHEt$_2$, 11%), indicating that NH hydrogen bonding does not significantly contribute to nonradiative deactivation in these systems. The π-extended pyrroles show noticeable solvatochromism, which we investigated in detail for the dipp-imide **4** (Figure 2C). For this system, it was found that on going from toluene to methanol, λ_{max}^{em} increases from 522 to 622 nm. As frequently observed in D–A fluorophores,[58] the strongest emission was observed in the least polar solvents ($\Phi_F \approx$ 23% in in toluene), and the quantum yields decreased considerably with increasing solvent polarity.

The bandgap difference between the diamide **2** and the diester **3** (λ_{max}^{abs} of 377 and 393 nm, respectively, $\Delta E = 0.13$ eV) is quite significant, and an even larger difference is observed between the emission maxima (0.39 eV). Inspection of the ground-state geometries of **2** and **3** reveals a difference of torsional angles of the carbonyl groups relative to the aromatic core. In the solid-state structure of **2** (Figures S21, S24), the amide groups take an antiparallel orientation, with the CCCO torsions relative to the naphthalene of ca. 52–53°. A slightly larger value (57.5°) was found in the DFT geometry of **2**. In the DFT geometry of **3**, the corresponding torsion is reduced to 36.3°, providing better conjugation of the ester substituents with the aromatic rings, and a reduction of the observed bandgap. The difference in CCCO torsions between **2** and **3** apparently originates from the larger steric requirements of the NMe$_2$ group relative to OMe. The different alignment of amide groups in **2** may be further stabilized by a tandem $n \rightarrow \pi^*$ interaction, similar to those observed in peptide chains.[59,60] This conjecture finds support in the increased pyramidalization ($\Delta = 0.034$ Å) of carbonyl carbons in **2** relative to those in **3** ($\Delta = 0.026$ Å, Figure S24). TD-DFT calculations predicted a significant reorganization of substituents in the S1 excited states of **2** and **3**. The S1 geometry of **2** is asymmetric (CCCO torsions of 61° and 37°), with a single enhanced $n \rightarrow \pi^*$ interaction ($\Delta = 0.052$ Å), whereas in the S1 state of **3**, the ester groups take a more coplanar position, with the CCCO torsions of 26°.

The conjugation is further improved upon planarization and subsequent π extension of the chromophore in derivatives **4–9**. The progression of red shifts in absorption and fluorescence spectra is however non-uniform, because several electronic effects contribute to the overall effect. For instance, in the imidazoles **6** and **7**, TD-DFT calculations show that the lowest-energy absorption band consists of two transitions (Figures S33, S34), each of which independently varies in its energy and oscillator strength in these two systems. Thus, even though λ_{max}^{abs} is larger for **7**, the actual bandgap is nearly identical in both derivatives, and the emission maximum of **6** is in fact slightly red shifted relative to that of **7**.
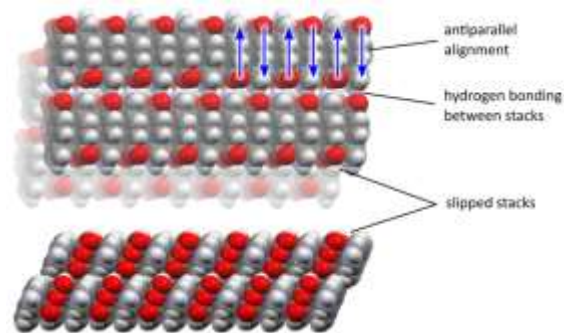
Figure 3. Crystal packing of **5** and intermolecular interactions observed in the solid state.

A consequence of the D–A design is the presence of large dipole moments in the molecules of pyrroles **2–9** (Chart 1), with a particularly large value calculated for the anhydride **5** (15.7 D). This feature is apparently responsible for the formation of antiparallel stacks in the solid-state structure of **5** (Figure 3). The resulting compensation of adjacent dipoles is a promising characteristic for applications in organic photovoltaic and transistor devices.[61–64] These stacks are only

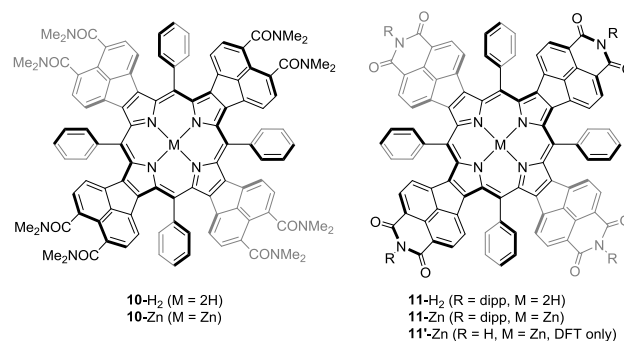slightly slipped (slip angle of 23°), and feature a small interplanar distance of 3.35 Å between consecutive molecules. The full coplanarity of all molecules in the crystal of **5** (i.e. the absence of herringbone packing) is expected to enable anisotropic electron transport along the π-stacking direction.[65] An additional enhancement of electron-transport properties may be provided by NH···O hydrogen bonds,[66,67] which form between adjacent stacks in one direction.

Porphyrins: Synthesis and Structure. To demonstrate the anticipated effect of pyrrole bandgap tuning on the electronic structure of higher-order systems, we chose to synthesize π-extended porphyrins **10**-M and **11**-M (Chart 2, M = 2H, Zn), bearing respectively naphthalene diamide (NDA) and naphthalene monoimide (NMI) units. These systems were envisaged as particularly attractive targets because of the inherently large red shifts observed for their electron-rich analogues,[49–53,55] and the soft character of the constituent chromophores,[68] which makes them susceptible to bandgap engineering.[52] *meso*-Aryl substitution was chosen with the expectation that the resulting macrocycles will be non-planar in analogy to *meso*-aryl acenaphthoporphyrins,[50,52] thus alleviating the solubility problems characteristic of their planar, *meso*-free congeners.[50]

The NDA-fused macrocycle was synthesized from the corresponding monopyrrole **2** under modified Lindsey conditions,[69] and isolated as the trifluoroacetate salt [**10**-H₄][TFA]₂ in a 42% yield. The efficiency of this condensation

Zn(OAc)₂. As a result, the expected **11**-Zn complex was obtained in an overall 87% yield. This procedure not only offers a more efficient alternative to direct pyrrole condensation, but also provides a general and concise route to variously N-substituted NMI-fused porphyrins.

Chart 2. π-Extended Electron-Deficient Porphyrins

10-H₂ (M = 2H)
10-Zn (M = Zn)

11-H₂ (R = dipp, M = 2H)
11-Zn (R = dipp, M = Zn)
11'-Zn (R = H, M = Zn, DFT only)

The ¹H NMR spectrum of **11**-H₂ revealed the presence of two nonequivalent sets of isopropyl substituents, consistent with the effective D_{2d} point symmetry and saddle-shaped curvature of the macrocycle. At 370 K, chemical exchange between the two *i*Pr groups was observed (ROESY, DMSO-d_6, 600 MHz), indicative of slow macrocyclic inversion. Solid-state (X-ray) and gas-phase (DFT) geometries of **11**-H₂ showed that the
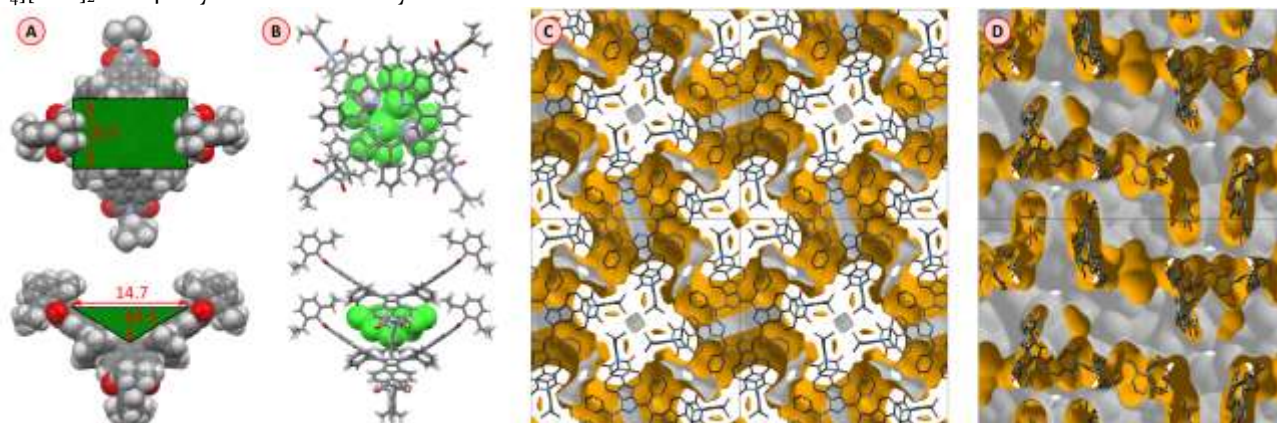

Figure 4. Solid-state structures of **11**-M. (**A**) Internal molecular free volume estimation in **11**-H₂. (**B**) Stacking along the *c* axis in the *I*–4 phase of **11**-H₂. Each void is occupied by ca. 2 disordered CHCl₃ molecules. Channel structures (procrystal electron density, 0.0003 au isosurface, solvent molecules removed for calculation) for the *I*–4 phase of **11**-H₂ (**C**, view along *c*) and *C*2/*c* phase of **11**-Zn (**D**, view along *a*). The interior of the channels is colored in gray.

reaction is particularly appreciable, given the electron-poor nature of the monopyrrole. The porphyrin salt, which can be made on a several hundred-milligram scale, was then converted into the corresponding free base and zinc(II) complex under standard conditions. The macrocyclization of **4** leading to the NMI system was not as efficient, providing only a 18% yield of **11**-H₂. The latter observation prompted the development of an indirect synthesis of the NMI target from the more easily accessible NDA porphyrin. To this end, [**10**-H₄][TFA]₂ was refluxed with concentrated hydrochloric acid to hydrolyze the amide groups. The resulting poorly soluble intermediate was investigated using MALDI and shown to consist of the corresponding octacarboxylic acid and anhydrides formed by its partial dehydration. This material was directly condensed with dipp-NH₂, and metalated with

molecule has a shape of a nanometer-sized tetrahedron, slightly flattened along the effective S_4 symmetry axis, with the distances between imidic nitrogens of 16.0 and 18.6 Å (solid state, 16.1 and 18.3 Å, DFT). The shape of the tetrahedron is essentially unaltered in the crystal structure of **11**-Zn; however, the NMR data obtained for the latter complex indicate that the barrier to inversion decreases upon metal binding. An earlier analysis of conformational dynamics of related acenaphthoporphyrins involved a mixture of *meso*-atropisomers and was not fully conclusive.[52]

The ¹H NMR spectrum of **10**-H₂ (CDCl₃, 300 K) is complicated by the partially restricted rotation of amide substituents, which leads to the formation of atropisomers. Fast rotation of amide groups relative to the aromatic core could however be observed at 410 K in DMSO-d_6 (600 MHz).

Because no suitable spectroscopic probe is present in **10**-H$_2$, its dynamics of inversion could not be monitored using NMR. However, the latter system is nevertheless expected to behave similarly to its imide analogue. In CDCl$_3$, the ^{1}H NMR spectrum of **10**-Zn reveals similar atropisomerism but is further complicated by aggregation, as judged by the unusually upfield shifts of selected signals.[70] The complexity of the spectrum precluded a detailed structural analysis, but we suppose that the formation of aggregates, which was not observed for **11**-Zn, is enhanced herein by intermolecular coordination of amide substituents to Zn centers in **10**-Zn.

The saddle-shaped distortion of the aromatic core in **11**-H$_2$ creates two shallow yet laterally extended cavities on the opposite sides of the macrocyclic surface. A conservative estimate of the internal molecular free volume (IMFV)[71,72] yields a value of ca. 600 Å^3 (Figure 4A). In contrast to triptycene (IMFV ≈ 93 Å^3), in which the voids are formed by three non-conjugated benzene rings, the cavities in **11**-H$_2$ are located within a contiguously conjugated π system that is deformed by steric effects. Flanked by the bulky dipp groups, the distorted core of **11**-H$_2$ does not support π-stacking in the solid-state, instead promoting the formation of intermolecular voids, which can enclathrate solvent molecules. In a tetragonal (*I*–4) crystal of **11**-H$_2$·*x*CHCl$_3$ (*x* ≈ 6), the saddles are stacked along the *c* axis (Figure 4B), with the *i*Pr groups resting on the naphthalene fragments of the neighboring molecules. Each of the intervening cavities tightly encapsulates an assembly of ca. two disordered chloroform molecules (additional CHCl$_3$ molecules are present in between the stacks).

Dispersion interactions involving the *i*Pr groups are also responsible for organizing the crystal packing in a monoclinic (*C*2/*c*) polymorph, **11**-M·*x*CH$_2$Cl$_2$·*y*C$_6$H$_{14}$ (*x* ≈ 2.25, *y* ≈ 5.75 for M = Zn; low-quality isomorphous crystals of **11**-H$_2$ were also obtained). The latter structure revealed a complex 3D system of channels, enclathrating disordered solvent molecules. These channels are permeable to spherical probes of up to 1.8 Å radius (Figure S27).[73] Calculations using the procrystal electron density method[74] performed for the solvent-free model of the *C*2/*c* phase showed that the voids occupy 31% of the cell volume. In the less solvated *I*–4 phase of **11**-H$_2$, the channels take up ca. 18% of the cell volume and have a permeability limit at a probe radius of ~1.3 Å. In the absence of strong intermolecular interactions, the crystals of **11**-Zn disintegrated rapidly on desolvation, and the remaining material was found to be effectively amorphous by powder X-ray diffraction. Nevertheless, the high solvation levels and channeled structures observed in the solid state indicate that with proper functionalization, such rigid non-planar aromatics may be usable for building extrinsically porous non-covalent frameworks.[75–78]

Porphyrins: Electronic Structure. The optical properties of **10**-M and **11**-M confirm the expected reduction of the electronic bandgap caused by fusion of electron deficient moieties. In particular, the absorption spectra of **10**-Zn and **11**-Zn show distinct red shifts relative to the spectrum of their naphthalene-unsubstituted analogue[52] (λ_{max}^{abs} = 558 and 672 nm for the lowest energy Soret and Q band, respectively). On going from **10**-Zn to **11**-Zn, the overall absorptivity increases, and the lowest-energy Q band experiences a red shift from 775 to 838 nm (Figure 5), corresponding to an apparent bandgap decrease of 0.12 eV. Likewise, the Soret band, which dominates

the visible part of the absorption spectrum, is shifted from 583 to 632 nm (Δ*E* = 0.16 eV), producing a dramatic color change (from violet to green). Thus, because of the unique position of the Soret bands,[68] the tuning of chromophore properties in **10**-Zn and **11**-Zn takes place simultaneously in the visible and NIR regimes. Both complexes showed weak fluorescence in the near IR range (Φ$_F$ ≈ 1%; λ_{max}^{em} = 806 and 893 nm for **10**-Zn to **11**-Zn, respectively). The red shifts of the optical spectrum induced in **11**-Zn by NMI fusion are very large and comparable with those previously achieved by *meso*-substitution and metalation of tetraacenaphthoporphyrin.[52] Since the latter method of optical tuning is complementary to the present D–A strategy, further reduction of bandgaps can be anticipated when these two approaches are used in conjunction.
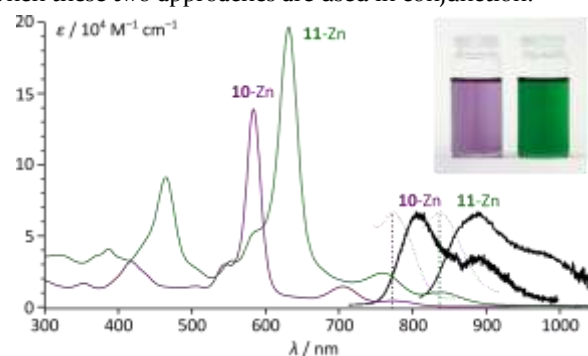

Figure 5. Electronic absorption spectra (~10 µM, colored traces) and fluorescence emission spectra (~5 µM, black traces) of **10**-Zn and **11**-Zn (toluene + 1% pyridine, 293 K).

The electron-withdrawing peripheries of **10**-Zn and **11**-Zn provide considerable stabilization of multiply charged anions. Using voltammetry, we were able to demonstrate six reduction waves for **10**-Zn, covering a range of potentials from −1.37 to −2.72 V vs. Fc+/Fc. Remarkably, eight chemically reversible reductions (−0.97 to −2.71 V) were recorded for the more electron-deficient **11**-Zn. The redox behavior of both porphyrins could be semi-quantitatively reproduced in a computational electrochemistry analysis, which gave roughly linear relationships between DFT-estimated absolute potentials and experimental values (Figure 6B). Our electrochemical results stand in sharp contrast with the behavior of zinc *meso*-tetratolylporphyrin, which can only accept two electrons under conventional experimental conditions,[79] and required a potential of ca. −3.7 V vs. Fc+/Fc to be charged to the hexaanion level.[80] Importantly, the parent monopyrrole (investigated in the N-substituted form **4**', Figure 6A) is also significantly more difficult to reduce than **11**-Zn. These observations indicate that the multi-charging capability only emerges from the combination of the two structural motifs, as a key benefit of our modular design.

The eightfold electrochemical reduction of **11**-Zn is a unique phenomenon, without a related precedent in the literature. Recognizing the relevance of the above finding, we next explored whether such highly charged species could also be generated by chemical reduction. To this end, titration of **11**-Zn with sodium anthracenide was followed spectrophotometrically in THF under strictly oxygen- and moisture-free conditions (Figure 7). The formation of eight consecutive species was identified in the course of the titration, but the individual forms were occasionally difficult to discern in the absence of clear isosbestic points. The analysis of the titration data was facilitated in a two-dimensional representation (Figure 7, bottom), in which specific absorption maxima could be more easily identified. Qualitatively, the reactivity induced by anthracenide is consistent with that observed electrochemically, and we propose that the species obtained by chemical reduction may indeed correspond to the [**11**-Zn]$^{n-}$ anions with n = 1 to 8. While the reported potential of sodium anthracenide (ca. −2.5

V relative to Fc+/Fc[81]) is too high to provide full coverage of the electrochemically determined reductions, the chemical charging of **11**-Zn can be assisted by the coordination of sodium to the resulting anions.[82]
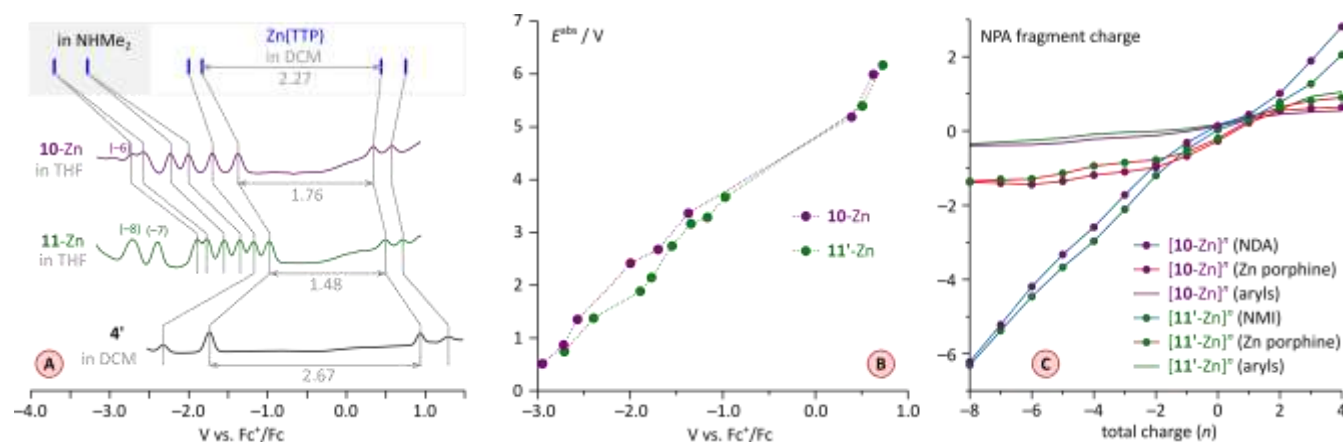

Figure 6. (**A**) Differential pulse voltammograms for **10**-Zn, **11**-Zn, and **4**' (THF, 0.1 M [NBu$_4$][BF$_4$], 293 K). Literature redox potentials for zinc(II) tetratolylporphyrin, Zn(TTP), in DCM and NHMe$_2$, have been re-referenced against the Fc+/Fc couple. (B) Relationship between DFT-estimated absolute redox potentials for **10**-Zn and **11**'-Zn (SMD(THF)/M06-2X/cc-VTZ//B3LYP/6-31G(d,p)) and experimental values determined for **10**-Zn and **11**-Zn, respectively. A weak chemically non-reversible wave at −2.95 V, observed for **10**-Zn, which might correspond to the 7th reduction is included in the graph. (**C**) NPA charge distribution for variously charged states of **10**-Zn and **11**'-Zn (M06-2X/cc-VTZ//B3LYP/6-31G(d,p)).
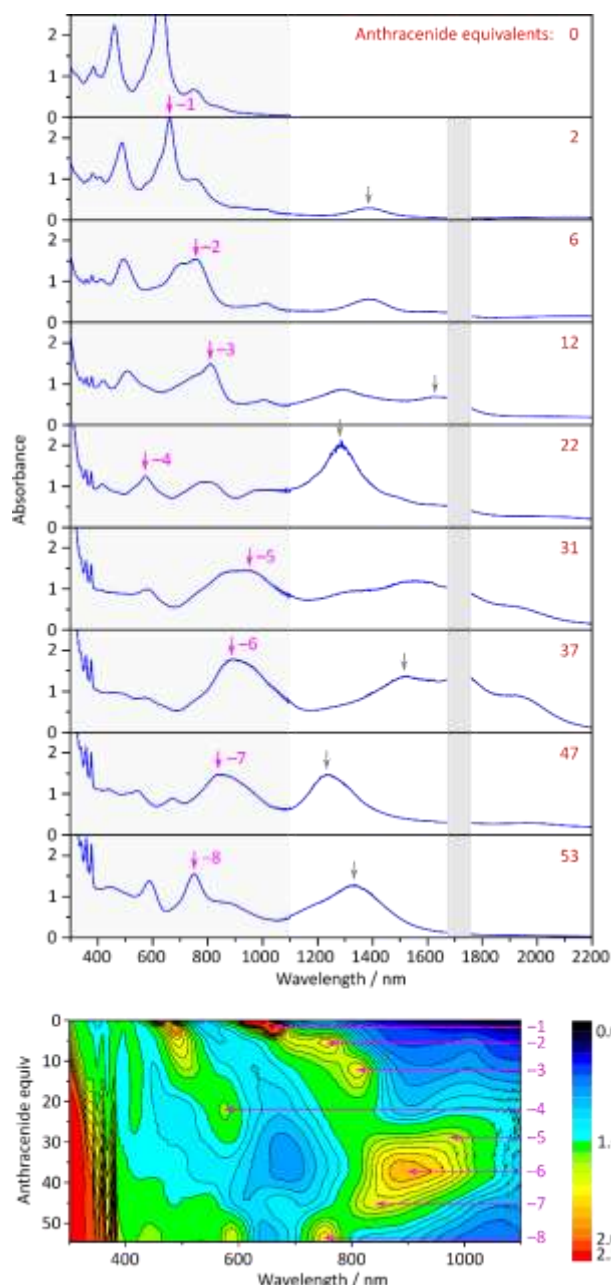
6

Figure 7. Titration of **11**-Zn (0.025 mM in THF) with sodium anthracenide. NIR absorptions in the 1100–2200 nm range were recorded in a separate experiment. The bottom panel shows the progress of titration as a 2D map, with a vertical resolution of 78 addition steps. Diagnostic maxima in the 300–1100 nm range, used for identification of consecutive species, and the expected charges are indicated with purple arrows in both panels. Additional maxima above 1100 nm are indicated with gray arrows.

The absorption spectra of the $[\textbf{11}\text{-Zn}]^{n-}$ anions show multiple broad bands of considerable intensity in the near infrared range. With the exception of $[\textbf{11}\text{-Zn}]^{8-}$, the absorptions extend beyond 2200 nm, indicating a dramatic reduction of the optical bandgaps relative to the neutral **11**-Zn (below 0.56 eV). The spectra do not have the typical porphyrin-like appearance, with clearly defined Soret- and Q-band regions. The π-electron conjugation in these anions is thus considerably perturbed relative to the neutral state, with

an apparent decrease of macrocyclic aromaticity. The anions absorb light in an unusually broad range of wavelengths, covering the UV, visible, and NIR regions, and the overall absorptivity remains high at all reduction stages (ε_{max} of 50000-100000 M^{-1} cm^{-1}). When these orbitals are partly filled upon reduction, the resulting electron configurations may indeed be expected to produce small optical bandgaps. **11**-Zn can thus be regarded as a redox-switchable panchromatic absorber with extended NIR activity. These optical features can be tentatively linked to small energy differences between the six lowest-lying virtual levels in the neutral **11**-Zn, all of which are characterized by considerable amplitudes on the NMI units (Figure S38).

Under completely inert conditions, the reduced forms of **11**-Zn are stable in solution. They are however immediately decomposed to unidentified products when exposed to air, and only $[\textbf{11}\text{-Zn}]^-$ could be transiently generated when traces of oxygen were present in solution. Nevertheless, when the presumed $[\textbf{11}\text{-Zn}]^{8-}$ was directly treated with excess I$_2$ in THF, ca. 90% of the initial **11**-Zn could be recovered (estimated spectrophotometrically). The latter experiment, which also required strict exclusion of oxygen, clearly demonstrates that the anthracenide-induced reduction of **11**-Zn has a generally reversible character.

Gas-phase geometries obtained for $[\textbf{10}\text{-Zn}]^n$ and $[\textbf{11}'\text{-Zn}]^n$ (n = −8 to +4, R = H for **11**') at the B3LYP/6-31G(d,p) level of theory are only weakly dependent on the overall oxidation level, although the saddle-like bending of the aromatic core increases for the most highly charged cations and anions. At this level of theory, di- and tetraanions of **10**-Zn and **11**'-Zn yielded broken-symmetry wavefunctions with nonzero $\langle S^2 \rangle$ values (Table S5), suggesting that a partial open-shell character can be anticipated for these anions. KS bandgaps calculated for cations and anions are considerably diminished relative to those of the neutral **10**-Zn and **11**'-Zn, in line with the results of reduction experiments presented above.

On the basis of simple π-electron count,[15] one might expect the even-electron $[\textbf{10}\text{-Zn}]^n$ and $[\textbf{11}'\text{-Zn}]^n$ species to alternately exhibit macrocyclic aromaticity (n = +4, 0, −4, −8) and antiaromaticity (n = +2, −2, −6). NICS(1) values calculated above the C$_3$N$_2$Zn ring centers for $[\textbf{11}'\text{-Zn}]^n$ (even n, ring A in Table S15) show that, in comparison with the neutral state (−10.7 ppm, strongly diatropic), the internal porphyrin ring currents are generally diminished upon charging (NICS(1) of 0.1 to −6.7 ppm at the C$_3$N$_2$Zn ring centers), with the exception of the dication $[\textbf{11}'\text{-Zn}]^{2+}$, which is predicted to be strongly paratropic (18.2 ppm). Simultaneously, the six-membered rings of naphthalene fragments retained negative values across the entire range of explored oxidation levels (−5.1 to −9.9 ppm). These results agree with the perceived loss of macrocyclic aromaticity, inferred from the absorption spectra of the anions.

The dependence of charge distribution in $[\textbf{10}\text{-Zn}]^n$ and $[\textbf{11}'\text{-Zn}]^n$ on the oxidation level (n = −8 to +4) was explored by means of natural population analysis (NPA, Figure 6C). On going from $[\textbf{10}\text{-Zn}]^0$ to $[\textbf{11}'\text{-Zn}]^0$, the total NPA charge on the Zn–porphine fragment increases from −0.27 to −0.20, in line with the increasing electron-accepting character of the peripheral units (NDA vs. NMI). It is however of interest that the peripheral moieties in neutral zinc porphyrins bear a positive charge, indicating a polarization reversal relative to monopyrroles. Nevertheless, upon reduction, these peripheral

fragments accept most of the incoming negative charge. The charge-storage capacity of the NMI units is higher in the initial reduction steps (n = –1 to –4), but it levels off at 79% of the total charge (over 6 charge units) in both systems for n = –8.

Charging a contiguously π-conjugated moiety beyond the tetraanion stage is generally difficult, especially in unsubstituted hydrocarbons.[83] Available data indicate that the charging capacity of π systems does not increase linearly with their size. Highest charge densities per non-H atom of –0.20 to –0.25 were reported for tetraanions of pyrene,[84] perylene,[84] acepleiadylene[85] tetradehydro[18]annulene,[86] and corannulene,[87–89] which typically benefit from aromatic stabilization and countercation coordination (notably Li). Peripheral imide groups assist in delocalization of negative charge, and a heptaanion was electrochemically generated for N-type nanoribbons containing 8 imide groups.[90] The latter design produced a much lower charge-per-atom density of –0.058. As the charge delocalization in **11**-Zn is mostly confined to the porphyrin–NMI core consisting of 84 non-H atoms (excluding Zn), the charging capacity is ca. 0.095 electron per atom at the octaanion level. In comparison, electron-deficient poly(quinoxaline) films could be charged electrochemically to ca. 0.25 e/subunit (0.025 electron per atom).[91] Overall, the porphyrin–NMI combination present in **11**-Zn emerges as an efficient means of storing multiple negative charges in a relatively small π-conjugated manifold.

CONCLUSIONS

The present work demonstrates a monomer-based approach to bandgap engineering, with potentially wide-ranging applications in oligopyrrole chemistry. In particular, we have shown the first example of a synthetically useful library of tunable pyrrole monomers, and the effective transferability of bandgap changes to oligopyrrole derivatives. In our donor–acceptor design, the five-membered ring at the junction between the pyrrole donor and the naphthalene acceptor ensures efficient π-conjugation, and has a potential for creating soft (easily tunable) chromophores,[68] as well as organic materials with a small reorganization energy.[92] The modular character of our approach offers the advantage of rapid elaboration of complex structures and the possibility of juxtaposing different D–A units as an additional means of bandgap control. Some of the acceptor groups introduced on the D–A monomers, notably the imide group, can be easily functionalized and also act as H-bonded elements[66,67,93–96] stabilizing supramolecular assemblies. The electron-deficient monopyrroles presented herein can further be viewed as unprecedented "umpolung" analogues of TTF-pyrrole,[97] with reversed dipole orientations and comparable synthetic utility.[98–100]

The multi-charging capability shown here for the NMI- and NDA-bearing porphyrins is a rare phenomenon in non-fullerene aromatics, with few systems capable of four or more reductions.[101–104] **11**-Zn is apparently the first non-oligomeric π-conjugated system for which a sequence of eight reversible reductions is reported. Further optimization of such electron-deficient porphyrins, which can be achieved by metal choice, peripheral substitution, geometry changes etc., may lead to even higher charge-per-atom densities at easily accessible potentials, making such materials of interest in charge storage applications. Simultaneously, the favorably positioned LUMO level makes these new systems of potential interest as acceptor

layers in bulk heterojunction photovoltaics.[105] In addition, the high nonplanarity combined with uninterrupted π conjugation in these macrocycles may provide access to extensively conjugated 3D systems, which, depending on the specific design, can reveal either intrinsic or extrinsic porosity. Most importantly, however, the structural paradigm employed here for the development of porphyrins is likely to be applicable to other classes of oligopyrroles. Efforts to explore these possibilities in various pyrrole-containing chromophores are currently underway.

ASSOCIATED CONTENT

Supporting Information

Experimental procedures and analytical data for all new compounds. Additional NMR and mass spectra, photoluminescence and electrochemistry data. X-ray data for **2**, **5**, **11**-H$_2$, and **11**-Zn (CIF). Computational data tables, figures, and Cartesian coordinates (PDB).

AUTHOR INFORMATION

Corresponding Author

* marcin.stepien@chem.uni.wroc.pl
Notes
The authors declare no competing financial interests.

ACKNOWLEDGMENT

REFERENCES

(1) Narita, A.; Wang, X.-Y.; Feng, X.; Müllen, K. *Chem. Soc. Rev.* **2015**, *44*, 6616–6643.
(2) Stępień, M.; Gońka, E.; Żyła, M.; Sprutta, N. *Chem. Rev.* **2016**, DOI 10.1021/acs.chemrev.6b00076.
(3) Li, C.; Liu, M.; Pschirer, N. G.; Baumgarten, M.; Müllen, K. *Chem. Rev.* **2010**, *110*, 6817–6855.
(4) Müllen, K. *ACS Nano* **2014**, *8*, 6531–6541.
(5) Zhu, X.; Tsuji, H.; López Navarrete, J. T.; Casado, J.; Nakamura, E. *J. Am. Chem. Soc.* **2012**, *134*, 19254–19259.
(6) Morales-Vidal, M.; Boj, P. G.; Villalvilla, J. M.; Quintana, J. A.; Yan, Q.; Lin, N.-T.; Zhu, X.; Ruangsupapichat, N.; Casado, J.; Tsuji, H.; Nakamura, E.; Díaz-García, M. A. *Nat. Commun.* **2015**, *6*, 8458.
(7) Li, Y.; Gao, J.; Di Motta, S.; Negri, F.; Wang, Z. *J. Am. Chem. Soc.* **2010**, *132*, 4208–4213.
(8) Yuan, Z.; Lee, S.-L.; Chen, L.; Li, C.; Mali, K. S.; De Feyter, S.; Müllen, K. *Chem. – Eur. J.* **2013**, *19*, 11842–11846.
(9) Zeng, Z.; Lee, S.; Zafra, J. L.; Ishida, M.; Zhu, X.; Sun, Z.; Ni, Y.; Webster, R. D.; Li, R.-W.; López Navarrete, J. T.; Chi, C.; Ding, J.; Casado, J.; Kim, D.; Wu, J. *Angew. Chem. Int. Ed.* **2013**, *52*, 8561–8565.
(10) Tsuda, A.; Osuka, A. *Science* **2001**, *293*, 79–82.
(11) Tanaka, T.; Osuka, A. *Chem. Soc. Rev.* **2015**, *44*, 943–969.
(12) Yoshii, R.; Yamane, H.; Tanaka, K.; Chujo, Y. *Macromolecules* **2014**, *47*, 3755–3760.
(13) Shin, J.-Y.; Furuta, H.; Yoza, K.; Igarashi, S.; Osuka, A. *J. Am. Chem. Soc.* **2001**, *123*, 7190–7191.

(14) Köhler, T.; Seidel, D.; Lynch, V.; Arp, F. O.; Ou, Z.; Kadish, K. M.; Sessler, J. L. *J. Am. Chem. Soc.* **2003**, *125*, 6872–6873.

(15) Stępień, M.; Sprutta, N.; Latos-Grażyński, L. *Angew. Chem. Int. Ed.* **2011**, *50*, 4288–4340.

(16) Hagberg, D. P.; Marinado, T.; Karlsson, K. M.; Nonomura, K.; Qin, P.; Boschloo, G.; Brinck, T.; Hagfeldt, A.; Sun, L. *J. Org. Chem.* **2007**, *72*, 9550–9556.

(17) Kivala, M.; Diederich, F. *Acc. Chem. Res.* **2009**, *42*, 235–248.

(18) Li, C.; Schöneboom, J.; Liu, Z.; Pschirer, N. G.; Erk, P.; Herrmann, A.; Müllen, K. *Chem. – Eur. J.* **2009**, *15*, 878–884.

(19) Achelle, S.; Barsella, A.; Baudequin, C.; Caro, B.; Robin-le Guen, F. *J. Org. Chem.* **2012**, *77*, 4087–4096.

(20) Zöphel, L.; Enkelmann, V.; Müllen, K. *Org. Lett.* **2013**, *15*, 804–807.

(21) Li, H.; Kim, F. S.; Ren, G.; Hollenbeck, E. C.; Subramaniyan, S.; Jenekhe, S. A. *Angew. Chem. Int. Ed.* **2013**, *52*, 5513–5517.

(22) van Mullekom, H. A. M.; Vekemans, J. A. J. M.; Havinga, E. E.; Meijer, E. W. *Mater. Sci. Eng. R Rep.* **2001**, *32*, 1–40.

(23) Beaujuge, P. M.; Amb, C. M.; Reynolds, J. R. *Acc. Chem. Res.* **2010**, *43*, 1396–1407.

(24) Zhang, Z.-G.; Wang, J. *J. Mater. Chem.* **2012**, *22*, 4178–4187.

(25) Li, H.; Kim, F. S.; Ren, G.; Jenekhe, S. A. *J. Am. Chem. Soc.* **2013**, *135*, 14920–14923.

(26) Chen, L.; Li, C.; Müllen, K. *J. Mater. Chem. C* **2014**, *2*, 1938–1956.

(27) Jiang, W.; Li, Y.; Wang, Z. *Acc. Chem. Res.* **2014**, *47*, 3135–3147.

(28) Würthner, F.; Saha-Möller, C. R.; Fimmel, B.; Ogi, S.; Leowanawat, P.; Schmidt, D. *Chem. Rev.* **2015**, *116*, 962–1052.

(29) Suraru, S.-L.; Würthner, F. *Angew. Chem. Int. Ed.* **2014**, *53*, 7428–7448.

(30) Jänsch, D.; Li, C.; Chen, L.; Wagner, M.; Müllen, K. *Angew. Chem. Int. Ed.* **2015**, *54*, 2285–2289.

(31) Suraru, S.-L.; Zschieschang, U.; Klauk, H.; Würthner, F. *Chem. Commun.* **2011**, *47*, 11504–11506.

(32) Würthner, F.; Ahmed, S.; Thalacker, C.; Debaerdemaeker, T. *Chem. – Eur. J.* **2002**, *8*, 4742–4750.

(33) Thalacker, C.; Röger, C.; Würthner, F. *J. Org. Chem.* **2006**, *71*, 8098–8105.

(34) Katz, H. E.; Lovinger, A. J.; Johnson, J.; Kloc, C.; Siegrist, T.; Li, W.; Lin, Y.-Y.; Dodabalapur, A. *Nature* **2000**, *404*, 478–481.

(35) Schneebeli, S. T.; Frasconi, M.; Liu, Z.; Wu, Y.; Gardner, D. M.; Strutt, N. L.; Cheng, C.; Carmieli, R.; Wasielewski, M. R.; Stoddart, J. F. *Angew. Chem. Int. Ed.* **2013**, *52*, 13100–13104.

(36) Loudet, A.; Burgess, K. *Chem. Rev.* **2007**, *107*, 4891–4932.

(37) Wood, T. E.; Thompson, A. *Chem. Rev.* **2007**, *107*, 1831–1861.

(38) Sessler, J. L.; Aguilar, A.; Sanchez-Garcia, D.; Seidel, D.; Köhler, T.; Arp, F.; Lynch, V. M. *Org. Lett.* **2005**, *7*, 1887–1890.

(39) Gońka, E.; Myśliwiec, D.; Lis, T.; Chmielewski, P. J.; Stępień, M. *J. Org. Chem.* **2013**, *78*, 1260–1265.

(40) Kadish, K. M.; Smith, K. M.; Guilard, R. *Handbook of Porphyrin Science*; World Scientific Publishing: Singapore; Vol. 1–35.

(41) Takase, M.; Enkelmann, V.; Sebastiani, D.; Baumgarten, M.; Müllen, K. *Angew. Chem. Int. Ed.* **2007**, *46*, 5524–5527.

(42) Takase, M.; Narita, T.; Fujita, W.; Asano, M. S.; Nishinaga, T.; Benten, H.; Yoza, K.; Müllen, K. *J. Am. Chem. Soc.* **2013**, *135*, 8031–8040.

(43) Gońka, E.; Chmielewski, P. J.; Lis, T.; Stępień, M. *J. Am. Chem. Soc.* **2014**, *136*, 16399–16410.

(44) Żyła, M.; Gońka, E.; Chmielewski, P. J.; Cybińska, J.; Stępień, M. *Chem. Sci.* **2016**, *7*, 286–294.

(45) Heinze, J.; Frontana-Uribe, B. A.; Ludwigs, S. *Chem. Rev.* **2010**, *110*, 4724–4771.

(46) Jiao, C.; Huang, K.-W.; Chi, C.; Wu, J. *J. Org. Chem.* **2011**, *76*, 661–664.

(47) Jiao, C.; Zu, N.; Huang, K.-W.; Wang, P.; Wu, J. *Org. Lett.* **2011**, *13*, 3652–3655.

(48) Jiao, C.; Huang, K.-W.; Wu, J. *Org. Lett.* **2011**, *13*, 632–635.

(49) Chandrasekar, P.; Lash, T. D. *Tetrahedron Lett.* **1996**, *37*, 4873–4876.

(50) Lash, T. D.; Chandrasekar, P. *J. Am. Chem. Soc.* **1996**, *118*, 8767–8768.

(51) Ono, N.; Hironaga, H.; Ono, K.; Kaneko, S.; Murashima, T.; Ueda, T.; Tsukamura, C.; Ogawa, T. *J. Chem. Soc. [Perkin 1]* **1996**, No. 5, 417–423.

(52) Spence, J. D.; Lash, T. D. *J. Org. Chem.* **2000**, *65*, 1530–1539.

(53) Ono, N.; Yamamoto, T.; Shimada, N.; Kuroki, K.; Wada, M.; Utsunomiya, R.; Yano, T.; Uno, H.; Murashima, T. *Heterocycles* **2003**, *61*, 433–447.

(54) Okujima, T.; Ando, C.; Mack, J.; Mori, S.; Hisaki, I.; Nakae, T.; Yamada, H.; Ohara, K.; Kobayashi, N.; Uno, H. *Chem. – Eur. J.* **2013**, *19*, 13970–13978.

(55) Ono, N.; Tsukamura, C.; Nomura, Y.; Hironaga, H.; Murashima, T.; Ogawa, T. *Adv. Mater.* **1997**, *9*, 149–153.

(56) Johnstone, K. D.; Pearce, W. A.; Pyke, S. M. *J. Porphyr. Phthalocyanines* **2002**, *6*, 661–672.

(57) Zhou, Y.; Xiao, Y.; Chi, S.; Qian, X. *Org. Lett.* **2008**, *10*, 633–636.

(58) Singha, S.; Kim, D.; Roy, B.; Sambasivan, S.; Moon, H.; Rao, A. S.; Kim, J. Y.; Joo, T.; Park, J. W.; Rhee, Y. M.; Wang, T.; Kim, K. H.; Shin, Y. H.; Jung, J.; Ahn, K. H. *Chem. Sci.* **2015**, *6*, 4335–4342.

(59) Newberry, R. W.; VanVeller, B.; Guzei, I. A.; Raines, R. T. *J. Am. Chem. Soc.* **2013**, *135*, 7843–7846.

(60) Wilhelm, P.; Lewandowski, B.; Trapp, N.; Wennemers, H. *J. Am. Chem. Soc.* **2014**, *136*, 15829–15832.

(61) Miao, Q.; Lefenfeld, M.; Nguyen, T.-Q.; Siegrist, T.; Kloc, C.; Nuckolls, C. *Adv. Mater.* **2005**, *17*, 407–412.

(62) Huang, L.; Stolte, M.; Bürckstümmer, H.; Würthner, F. *Adv. Mater.* **2012**, *24*, 5750–5754.

(63) Arjona-Esteban, A.; Krumrain, J.; Liess, A.; Stolte, M.; Huang, L.; Schmidt, D.; Stepanenko, V.; Gsänger, M.; Hertel, D.; Meerholz, K.; Würthner, F. *J. Am. Chem. Soc.* **2015**, *137*, 13524–13534.

(64) Dou, J.-H.; Zheng, Y.-Q.; Yao, Z.-F.; Yu, Z.-A.; Lei, T.; Shen, X.; Luo, X.-Y.; Sun, J.; Zhang, S.-D.; Ding, Y.-F.; Han, G.; Yi, Y.; Wang, J.-Y.; Pei, J. *J. Am. Chem. Soc.* **2015**, *137*, 15947–15956.

(65) Dong, H.; Fu, X.; Liu, J.; Wang, Z.; Hu, W. *Adv. Mater.* **2013**, *25*, 6158–6183.

(66) Black, H. T.; Perepichka, D. F. *Angew. Chem. Int. Ed.* **2014**, *53*, 2138–2142.

(67) Black, H. T.; Lin, H.; Bélanger-Gariépy, F.; Perepichka, D. F. *Faraday Discuss.* **2014**, *174*, 297–312.

(68) Mack, J.; Asano, Y.; Kobayashi, N.; Stillman, M. J. *J. Am. Chem. Soc.* **2005**, *127*, 17697–17711.

(69) Lindsey, J. S. *Acc. Chem. Res.* **2010**, *43*, 300–311.

(70) Myśliwiec, D.; Donnio, B.; Chmielewski, P. J.; Heinrich, B.; Stępień, M. *J. Am. Chem. Soc.* **2012**, *134*, 4822–4833.

(71) Long, T. M.; Swager, T. M. *Adv. Mater.* **2001**, *13*, 601–604.

(72) Tsui, N. T.; Paraskos, A. J.; Torun, L.; Swager, T. M.; Thomas, E. L. *Macromolecules* **2006**, *39*, 3350–3358.

(73) Barbour, L. J. *Chem. Commun.* **2006**, No. 11, 1163.

(74) Turner, M. J.; McKinnon, J. J.; Jayatilaka, D.; Spackman, M. A. *CrystEngComm* **2011**, *13*, 1804–1813.

(75) McKeown, N. B.; Makhseed, S.; Msayib, K. J.; Ooi, L.-L.; Helliwell, M.; Warren, J. E. *Angew. Chem. Int. Ed.* **2005**, *44*, 7546–7549.

(76) Mastalerz, M.; Oppel, I. M. *Angew. Chem. Int. Ed.* **2012**, *51*, 5252–5255.

(77) Chen, T.-H.; Popov, I.; Kaveevivitchai, W.; Chuang, Y.-C.; Chen, Y.-S.; Daugulis, O.; Jacobson, A. J.; Miljanić, O. Š. *Nat. Commun.* **2014**, *5*, 5131.

(78) Slater, A. G.; Cooper, A. I. *Science* **2015**, *348*, aaa8075.

(79) Kumar, P. P.; Maiya, B. G. *New J. Chem.* **2003**, *27*, 619–625.

(80) Cosmo, R.; Kautz, C.; Meerholz, K.; Heinze, J.; Müllen, K. *Angew. Chem. Int. Ed. Engl.* **1989**, *28*, 604–607.

(81) Connelly, N. G.; Geiger, W. E. *Chem. Rev.* **1996**, *96*, 877–910.

(82) Reed, C. A. In *Electrochemical and Spectrochemical Studies of Biological Redox Components*; Advances in Chemistry; American Chemical Society: Washington, D.C., 1982; Vol. 201, pp 333–356.

(83) Müllen, K. *Chem. Rev.* **1984**, *84*, 603–646.

(84) Minsky, A.; Meyer, A. Y.; Rabinovitz, M. *J. Am. Chem. Soc.* **1982**, *104*, 2475–2482.

9

(85) Becker, B. C.; Huber, W.; Müllen, K. *J. Am. Chem. Soc.* **1980**, *102*, 7803–7805.

(86) Müllen, K.; Huber, W.; Meul, T.; Nakagawa, M.; Iyoda, M. *J. Am. Chem. Soc.* **1982**, *104*, 5403–5411.

(87) Ayalon, A.; Rabinovitz, M.; Cheng, P.-C.; Scott, L. T. *Angew. Chem. Int. Ed. Engl.* **1992**, *31*, 1636–1637.

(88) Baumgarten, M.; Gherghel, L.; Wagner, M.; Weitz, A.; Rabinovitz, M.; Cheng, P.-C.; Scott, L. T. *J. Am. Chem. Soc.* **1995**, *117*, 6254–6257.

(89) Zabula, A. V.; Filatov, A. S.; Spisak, S. N.; Rogachev, A. Y.; Petrukhina, M. A. *Science* **2011**, *333*, 1008–1011.

(90) Zhen, Y.; Wang, C.; Wang, Z. *Chem. Commun.* **2010**, *46*, 1926–1928.

(91) Yamamoto, T.; Sugiyama, K.; Kushida, T.; Inoue, T.; Kanbara, T. *J. Am. Chem. Soc.* **1996**, *118*, 3930–3937.

(92) Chen, W.-C.; Chao, I. *J. Phys. Chem. C* **2014**, *118*, 20176–20183.

(93) Houlton, A.; Michael, D.; Mingos, P.; Williams, D. J. *Transit. Met. Chem.* **1994**, *19*, 653–656.

(94) Bishop, M. M.; Lindoy, L. F.; Turner, P. *Supramol. Chem.* **2002**, *14*, 179–188.

(95) Bishop, M. M.; Coles, S. J.; Lindoy, L. F.; Parkin, A. *Inorganica Chim. Acta* **2006**, *359*, 3565–3580.

(96) McMorran, D. A.; McAdam, C. J.; Salm, H. van der; Gordon, K. C. *Dalton Trans.* **2013**, *42*, 2948–2962.

(97) Jeppesen, J. O.; Takimiya, K.; Jensen, F.; Becher, J. *Org. Lett.* **1999**, *1*, 1291–1294.

(98) Becher, J.; Brimert, T.; Jeppesen, J. O.; Pedersen, J. Z.; Zubarev, R.; Bjørnholm, T.; Reitzel, N.; Jensen, T. R.; Kjaer, K.; Levillain, E. *Angew. Chem. Int. Ed.* **2001**, *40*, 2497–2500.

(99) Nielsen, K. A.; Cho, W.-S.; Jeppesen, J. O.; Lynch, V. M.; Becher, J.; Sessler, J. L. *J. Am. Chem. Soc.* **2004**, *126*, 16296–16297.

(100) Takase, M.; Yoshida, N.; Nishinaga, T.; Iyoda, M. *Org. Lett.* **2011**, *13*, 3896–3899.

(101) Naoda, K.; Mori, H.; Aratani, N.; Lee, B. S.; Kim, D.; Osuka, A. *Angew. Chem. Int. Ed.* **2012**, *51*, 9856–9859.

(102) Chou, C.-M.; Saito, S.; Yamaguchi, S. *Org. Lett.* **2014**, *16*, 2868–2871.

(103) Mori, H.; Tanaka, T.; Lee, S.; Lim, J. M.; Kim, D.; Osuka, A. *J. Am. Chem. Soc.* **2015**, *137*, 2097–2106.

(104) Zhang, G.; Lami, V.; Rominger, F.; Vaynzof, Y.; Mastalerz, M. *Angew. Chem. Int. Ed.* **2016**, *55*, 3977–3981.

(105) Anthony, J. E. *Chem. Mater.* **2011**, *23*, 583–590.